FRONTIERS OF PHYSICS

RESEARCH ARTICLE
Volume 19 / Issue 2 / 23204 / 2024

Nanophononic metamaterials induced proximity effect in heat flux regulation

Jian Zhang[1,2], Haochun Zhang[1,†], Gang Zhang[2,‡]

1 School of Energy Science and Engineering, Harbin Institute of Technology, Harbin 150001, China
2 Institute of High Performance Computing, Agency for Science, Technology and Research (A*STAR), Singapore 138632, Singapore
Corresponding authors. E-mail: †hczhang@hit.edu.cn, ‡zhangg@ihpc.a-star.edu.sg
Received August 27, 2023; accepted September 14, 2023

ABSTRACT

Recent studies have shown that the construction of nanophononic metamaterials can reduce thermal conductivity without affecting electrical properties, making them promising in many fields of application, such as energy conversion and thermal management. However, although extensive studies have been carried out on thermal conductivity reduction in nanophononic metamaterials, the local heat flux characteristic is still unclear. In this work, we construct a heat flux regulator which includes a silicon nanofilm with silicon pillars. The regulator has remarkable heat flux regulation ability, and various impacts on the regulation ability are explored. Surprisingly, even in the region without nanopillars, the local heat current is still lower than that in pristine silicon nanofilms, reduced by the neighboring nanopillars through the thermal proximity effect. We combine the analysis of the phonon participation ratio with the intensity of localized phonon modes to provide a clear explanation. Our findings not only provide insights into the mechanisms of heat flux regulation by nanophononic metamaterials, but also will open up new research directions to control local heat flux for a broad range of applications, including heat management, thermoelectric energy conversion, thermal cloak, and thermal concentrator.

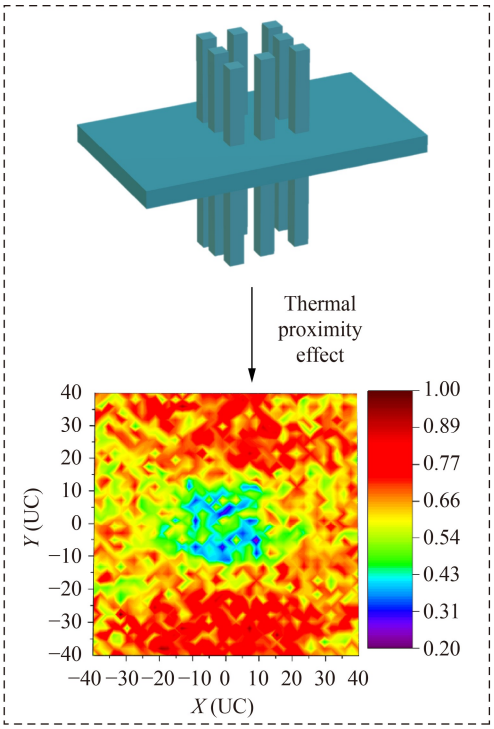

Keywords nanophononic metamaterials, proximity effect

1 Introduction

Electronic devices have become more power dense in recent decades, thus improving the control of thermal conduction at the nanoscale has become a topic of particular interest. In addition to thermal management, understanding thermal conduction on the nanoscale is also critical in other fields of application, such as thermoelectric energy conversion [1–3]. A great deal of potential has been demonstrated for controlling thermal conductivity by nanophononic metamaterials with artificial structures on the nanoscale in recent years. Nanophononic metamaterials have been shown to significantly reduce thermal conductivity in pillared thin films at nanoscale for the first time by Davis and Hussein [4]. In such a structure, there is strong resonance hybridization between phonons in the nanopillars and in the thin film, which results in a reduction in the group velocity of

Higher Education Press

https://doi.org/10.1007/s11467-023-1349-4

phonons [5]. Theoretical and simulation works demonstrate that the thermal conductivity is reduced by the flat hybridization bands induced by the nanopillars, combined with Bragg scattering when the nanopillars are arranged periodically [6–9]. In addition, Yudistira *et al.* [10] and Li *et al.* [11] designed GHz hypersonic nanophonon metamaterials based on nanoscale pillars, and also observed the local resonance hybridization effect.

A better knowledge of thermal conduction in nanophononic metamaterials definitely can facilitate their related applications. There have been numerous studies conducted on designing different nanophononic metamaterials and understanding the thermal conduction mechanism. Based on the phonon resonance hybridization mechanism, Wan *et al.* [12] designed graphene nanoribbons with pillared nanostructures to tune their thermal conductivity by isotope, which lead to a relative increase compared to the nominal nanophononic metamaterial configuration. Furthermore, Wang and co-workers [13] investigated the effects of imperfections on the thermal conductivity of graphene nanoribbons with pillared nanostructures. It was found that introducing imperfections can weaken the resonant hybridization strength as well as increase thermal conductivity. Aside from the reduction of thermal conductivity, it was found [5, 14] that in silicon thin films with surface nanostructured pillars, the in-plane thermal conductivity is anisotropic, although silicon is isotropic material. Hu and co-workers [15] studied the thermal conductivity of a silicon matrix with a germanium-nanoparticle array embedded and found similar flat hybridization bands in phonon dispersions. Zhang *et al.* [16] further designed a novel nanowire structure through a screw threadlike helical nanowall. In this structure, because the helical nanowall has a large contact area, it can result in strong resonance and a 36% reduction in thermal conductivity. Anderson localization of phonon propagation and remarkable reduction in thermal conductivity was also observed in aperiodic superlattices [17] and graded superlattices with short-range order [18]. In spite of studies that have improved the understanding of thermal conduction in nanophononic metamaterials [19–22], however, these previous works focused on the thermal conductivity of the whole structure. Although extensive studies have been carried out on thermal conductivity, the local heat flux characteristic is still unclear.

In this study, an example of a nanoscale phononic structure including a silicon nanofilm with silicon pillars is used to investigate the effects of nanoscale phononic metastructures on local heat current properties. Surprisingly, even in the region without nanopillars, the local heat current is still lower than that in pristine silicon nanofilms. In our molecular dynamics (MD) simulation, we combine the analysis of the phonon participation ratio with the spatial distribution of specific modes to provide a clear explanation. The present work would promote thermal engineering by localization via nanophononic metamaterials.

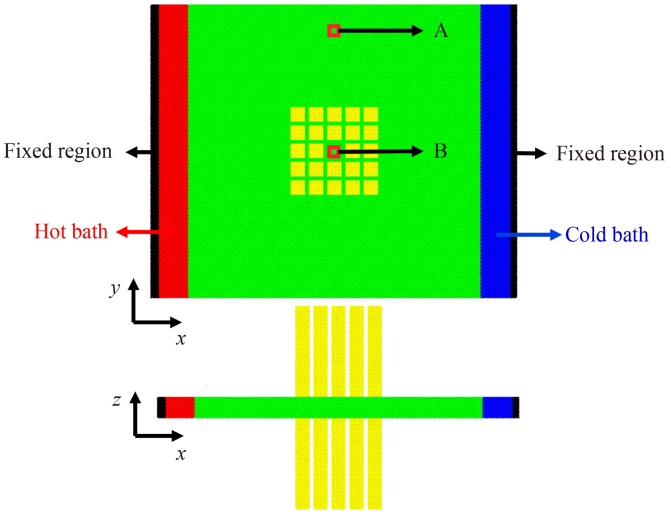

Fig. 1 The schematic of the configurations of the regulator, the functional region is constructed by nanopillars arranged periodically. Specific parameter information is shown in the main text.

2 Model and calculation method

The schematic of the configurations of the heat flux regulator is shown in Fig. 1. In the regulator, three regions are defined: the functional region (nanopillars-region), the pristine region far away from the functional region (A-region), and the region at the center of the functional region although no nanopillars existed in this region (B-region). Here, we adopt the non-equilibrium MD simulation to study the heat flux regulation of regulators using the LAMMPS packages [23]. In all MD simulations, to describe the interaction among Si atoms, Stillinger–Weber potential [24] is used. The whole system is firstly energy minimized, and then all atoms are given an initial velocity corresponding to 300 K which obeys the Gaussian distribution. They are relaxed in the canonical (constant atom number, volume, temperature, NVT) ensemble for 100 ps. Next, the atoms in the two ends (the fixed region in Fig. 1) are fixed. Here periodic boundary condition is applied along y- and z-direction (please refer to Fig. 1), fixed boundary condition is only applied along x-direction. A temperature gradient along the x-axis is established by placing atoms close to the two fixed regions into Nose–Hoover thermostats at 320 K and 280 K, respectively [See the Electronic Supplementary Materials (ESM)]. After that, molecular dynamics simulations are conducted for 2 ns to ensure that the system reaches a nonequilibrium steady state

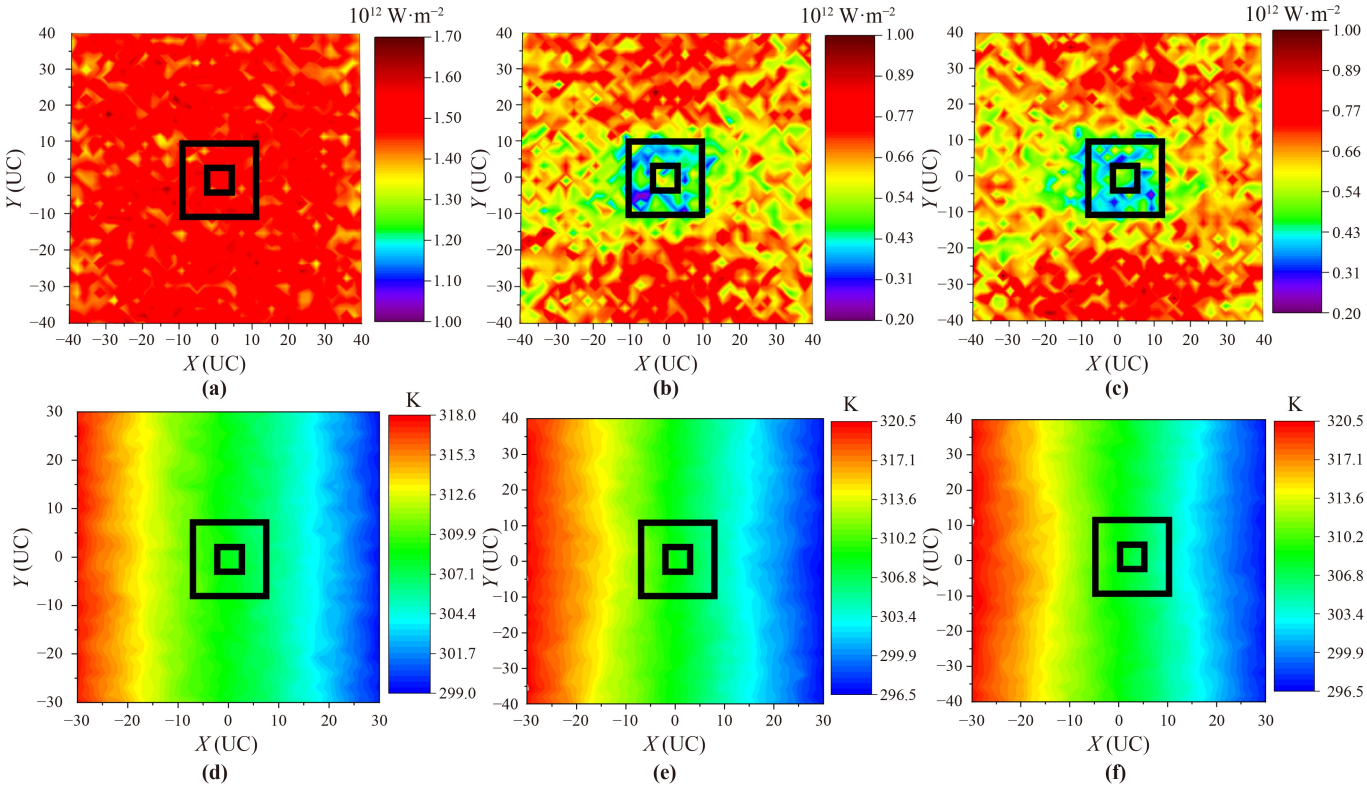

Fig. 2 Heat flux and temperature profiles of the regulators and pristine silicon films. **(a–c)** The heat flux profile, **(d–f)** the temperature profile. (a, d) The pristine silicon film, (b, e) the nanopillar height is 25 UC, and (c, f) the nanopillar height is 50 UC.

with a time-independent temperature gradient and heat flux. Detailed information on temperature and heat flux calculation can be found in the supplemental information.

We show the representative model configurations of suspended silicon nanofilms with surface nanoscale pillars in Fig. 1. Our nanofilms are created by cleaving bulk Si supercells in the direction of [001] to construct pristine surfaces. To construct the nanofilm, a Si cubic unit cell (UC) is replicated: the pristine nanofilm is made up of 6 UC (thickness), 100 UC (length), and 80 UC (width). For the regulator, the side width of the nanopillar is 4 × 4 UC, with a spacing of 1 UC, and tunable heights (25 and 50 UC). For comparison, the pristine silicon film is also considered. Except for the thermostat and the fixed regions, the system is divided into 40 × 40 small blocks to calculate heat flux and temperature profile.

3 Results and discussion

3.1 The heat flux proximity effect

Figure 2 illustrates the profile of temperature and heat flux. The pristine silicon nanofilm has a uniform distribution of temperature from the hot to the cold bath. In the pristine silicon film, the heat flux is distributed relatively uniformly along the x-axis. However, in the two regulators, local heat flux in the central regions is kept extremely low.

To quantitatively evaluate the ability of heat flux regulation, we calculate the local heat flux in regions A and B (as shown in Fig. 1) and define the ratio of heat flux (RHF) as RHF $= J_B/J_A$. As shown in Table 1, the RHF is 1 in the pristine silicon film and less than 1 for both regulators. Therefore, in the B-region, although no nanopillars exist in this region, its local heat flux is obvi-

Table 1 The ratio of heat flux with different regulators.

Film thickness (UC)	Nanopillar width (UC)	Nanopillar height (UC)	Nanopillar spacing (UC)	Number of nanopillars	The ratio of heat flux (RHF)
6	0	0	0	0	1
6	4	25	1	22	0.786
6	4	50	1	22	0.714

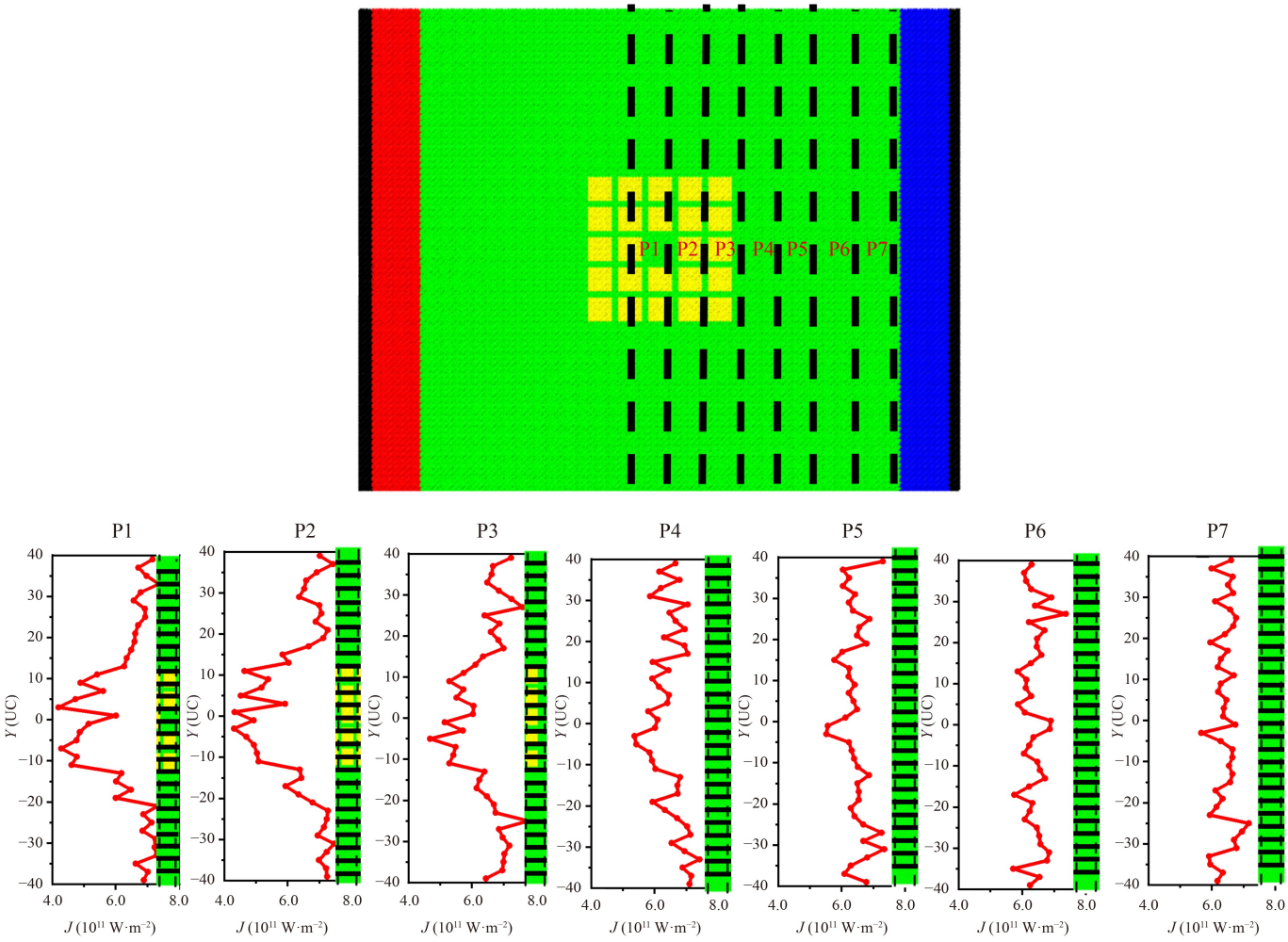

Fig. 3 The heat flux spatial distribution of the regulator in region P1–P7 with the nanopillar height is 50 UC.

ously lower than that of the pristine region. Moreover, with the height of the nanopillar increasing, the heat flux regulation efficiency increases. For example, when the height of the nanopillar increases from 25 to 50 UC, the RHF decreases from 0.786 to 0.714.

In previous theoretical and experimental reports [4–11], the nanophononic metastructure can induce an obvious reduction in thermal conductivity by the mechanisms of Bragg diffraction and phonon flat hybridization bands. However, here we find that in the region without nanopillars, local heat flux also can be reduced by the neighboring nanopillars, with such phenomenon having characteristics similar to the proximity effect. The ability to control heat flux locally has attracted extensive research interest in recent decades and based on transformation thermotics various thermal functional devices are proposed [25–27], including thermal cloak, thermal concentrator, and thermal rotator. In these thermal devices, inhomogeneous materials should be combined in a certain pattern, and even "negative" thermal conductivity may be required to realize the expected function. On the other side, in this work, the host silicon film is a homogeneous material, and the non-uniform heat flux distribution can be realized by surface coating with nanopillars. It is worth noting that in experiments, such nanopillars could be fabricated using vapor–liquid–solid processes [28], dry etching [29], and wet etching [30]. Therefore, the suggested configuration and heat flux control in our work may be achieved with existing nanotechnology.

Furthermore, we calculate the location-dependent heat flux distribution along the y-axis, in arrays P1–P7. Figure 3 shows the results of the regulator with the nanopillar height of 50 UC, and the results of the other structures are shown in the supplemental information. As shown in Fig. 3, in regions of P5–P7, the local heat flux along the y-axis is spatially homogeneously distributed. On the other side, in regions P2 & P3, the local heat flux in the central region is obviously lower than in the pristine section. The commonly accepted explanation of the mechanism behind the reduction is that nanophononic metastructure can induce flat phonon bands and strong Bragg diffraction [4–11].

However, in regions P1 & P4, particularly in P1,

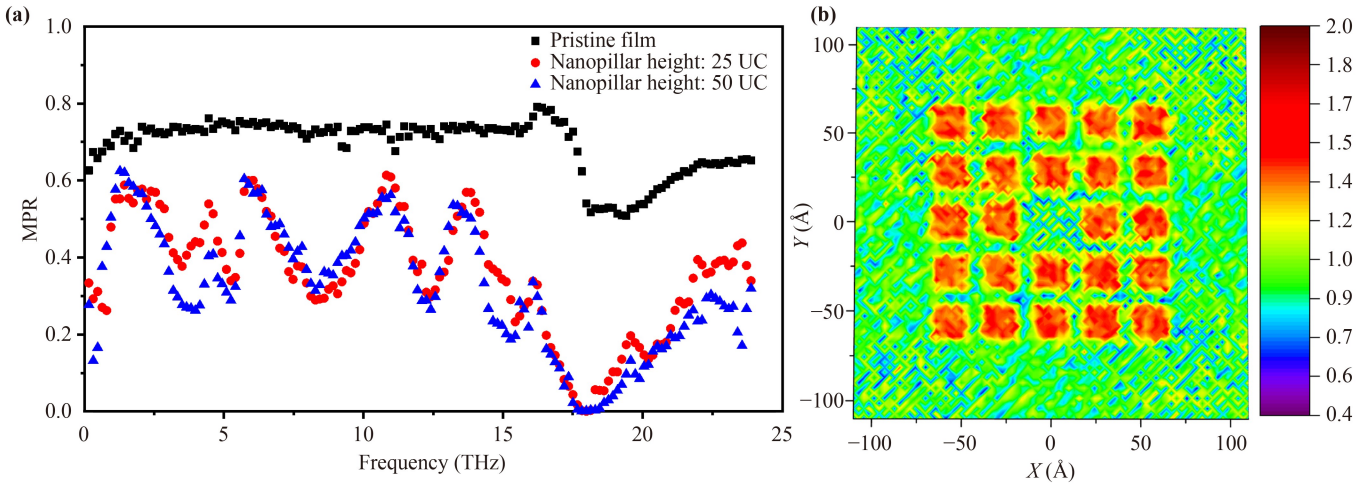

Fig. 4 **(a)** The mode participation rate of the regulators and pristine silicon nanofilm. **(b)** The intensity of localized phonon modes in regulator with the nanopillar height of 50 UC. The larger the value of the intensity of localized phonon modes, the lower the MPR.

compared with the pristine section, there is a dramatic reduction in local heat flux in the central part, although no nanopillars is existing there. Clearly, the nanopillars induce the heat flux proximity effect. Here we define the inhomogeneity ratio (α) $\alpha = J_{\mathrm{mid}}/J_{\mathrm{edge}}$, where J_{edge} is the average heat flux at the edges (–40 to –20 UC and 20 to 40 UC along the y direction, for details, please refer to Fig. 1) and J_{mid} is the average heat flux at the center (–10 to 10 UC along the y-axis). The heat flux at the center is 0.74 of that at the edges, indicating that the heat flux regulation is achieved due to the presence of the nanopillar around the studied section.

3.2 Phonon localization phenomenon

In this section, we use phonon localization theory to explore the underlying mechanism. In the different systems, we choose the same region (20 × 20 UC) adjacent to the nanopillars for calculating velocity autocorrelation, and the autocorrelation time is 30 ps. The Fourier transforms of velocity autocorrelation functions can be used to calculate the phonon density of states (PDOS) [31], as follows:

$$\mathrm{PDOS}\left(\omega\right) = \frac{1}{N\sqrt{2\pi}} \int \mathrm{e}^{-\mathrm{i}\omega t} \left\langle \sum_{j=1}^{N} \boldsymbol{v}_j\left(0\right) \boldsymbol{v}_j\left(t\right) \right\rangle \mathrm{d}t, \quad (1)$$

where ω is the phonon frequency, N is the number of atoms, and $\boldsymbol{v}$ is the velocity vector. The mode participation rate (MPR) is calculated based on the PDOS [32],

$$\mathrm{MPR}\left(\omega\right) = \frac{1}{N} \frac{\left[\sum_i \mathrm{PDOS}_i(\omega)^2\right]^2}{\sum_i \mathrm{PDOS}_i\left(\omega\right)^4}, \quad (2)$$

where $\mathrm{PDOS}_i\ (\omega)$ is the phonon density of states at specific atomic i locations according to Eq. (1).

As a measurement of the fraction of atoms involved in a particular mode, the mode participation rate can be used to determine the delocalized and localized modes, which provides detailed information on the effect of localization for each phonon mode. Figure 4(a) compares the mode participation rates of the two regulators with that of the pristine film. The mode participation rates of both low-frequency and high-frequency phonons are reduced in regulators compared with the pristine film. Most mode participation rates in the perfect films are higher than 0.5 and exhibit the characteristics of a delocalized nature, whereas the majority of mode participation rates in regulators are less than 0.5 and exhibit the characteristics of localized mode. Thus, the nanopillars region hinders phonon transport.

Furthermore, to obtain specific position information about phonon localization, we also calculate the intensity of localized phonon modes ($\Lambda \in \mathrm{MPR} < 0.4$) [33, 34]:

$$\phi_{i\alpha,\Lambda} = \frac{\int_{\Lambda} \mathrm{PDOS}_{i\alpha} \mathrm{d}\omega}{\frac{1}{N} \sum\limits_{1 \leqslant i \leqslant N} \int_{\Lambda} \mathrm{PDOS}_{i\alpha} \mathrm{d}\omega}, \quad (3)$$

where $\alpha = x$, y, and z. In the calculation, we average $\phi_{i\alpha}$ over all atoms with the same x/y and plot the distribution of the localized phonon modes in the xy-plane. We choose the same computational domain as presented in Fig. 4(a). Figure 4(b) shows the intensity of localized phonon modes in the regulator with the nanopillar height is 50 UC. The results of the other regulators are shown in the supplemental information. In general, a higher value of $\phi_{i\alpha}$ means a stronger localization of the phonon mode at the ith atom. It is clear that the localized modes are distributed in the functional region, and it is

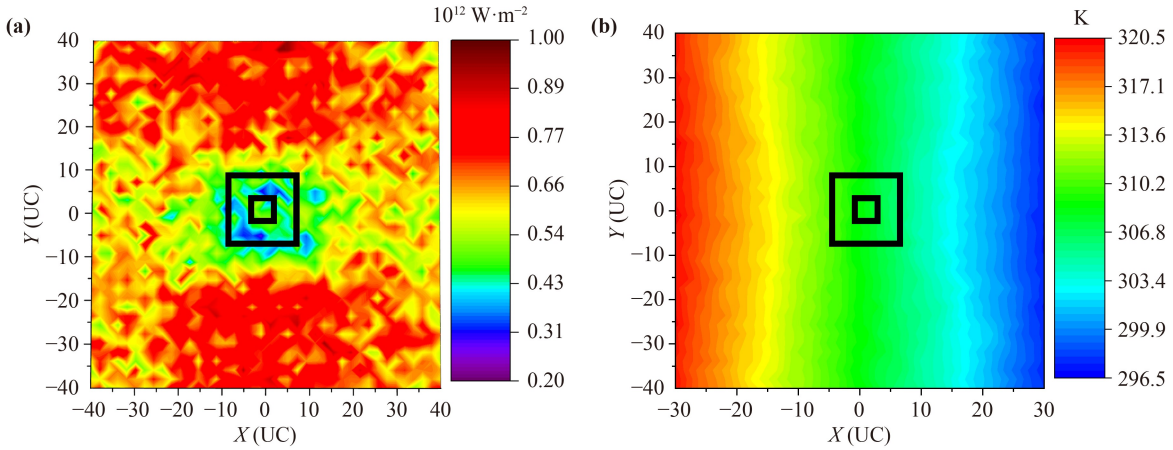

Fig. 5 The heat flux **(a)** and temperature **(b)** profile of the regulator when the host nanofilm thickness is 10 UC.

low in the pristine region and even in the center of the functional region. In the calculation of intensity of localized phonon modes, only the base film is considered, and the low MPR is due to the local resonance effect between the nanopillars and the base film. These results provide a direct demonstration that localization takes place within the functional regions. Although there is no obvious localization mode in the central region, its local heat flux is significantly reduced due to the proximity effect induced by the nanopillar region.

3.3 Impact of the thickness of host nanofilm

Hossein *et al.* [5] found that the height of the nanopillars, their spacing, and the arrangement of the inhomogeneous height, have significant effects on the thermal conductivity. In this section, we investigate the effect of host nanofilm thickness on the ability of the regulator to tune heat flux. We choose a regulator with the nanopillar height is 25 UC (as discussed in Section 3.1) and increase the host nanofilm thickness to 10 UC. Figure 5 illustrates the temperature and heat flux profiles. In the regulator, local heat flux in the central regions is kept extremely low. In addition, its RHF is 0.824, which is higher than the regulator with host nanofilm thickness of 6 UC. We present the spatial distribution of heat flux in P1–P7 in Fig. S4 of the ESM. The heat flux in the center gradually increases from P1 to P7, and the inhomogeneity ratio in section P1 is 0.82, which is also higher than the regulator with host nanofilm thickness of 6 UC. We speculate that this is due to the weakened localization of the host nanofilm due to the increased film thickness. Therefore, increasing the thickness of the host nanofilm can suppress the heat flux regulation ability.

3.4 Impact of the number of nanopillars

In the previous section, we investigate the effect of host nanofilm thickness on the ability to regulate heat flux. In this section, we fix the thickness of host nanofilm as 6 UC, and the height of nanopillars is 25 UC, while reduce

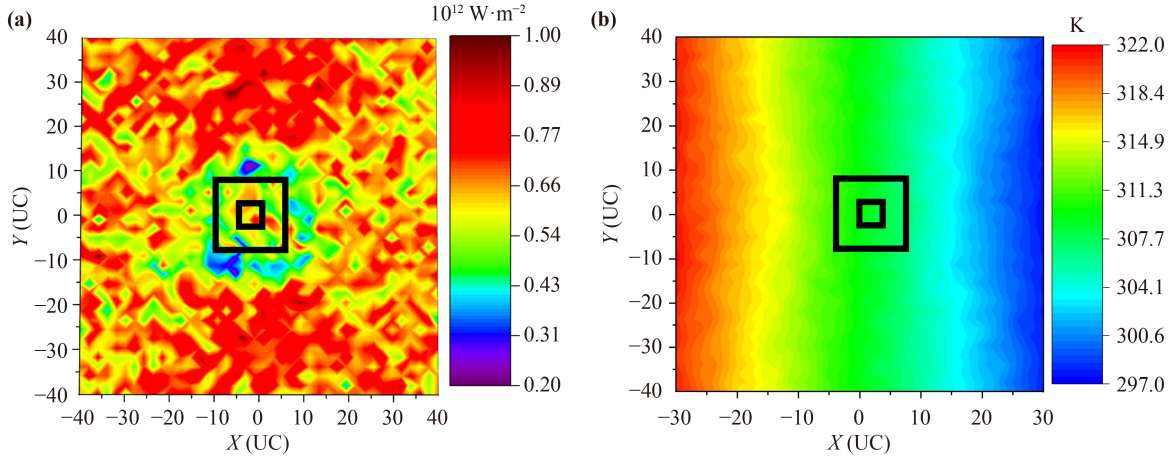

Fig. 6 The heat flux **(a)** and temperature **(b)** profile of the regulator with the nanopillar row is 1.

the number of nanopillars from 22 to 16 to study its impact on heat flux regulation ability. Figure 6 illustrates the temperature and heat flux profile. Overall, local heat flux in the functional regions is kept extremely low, demonstrating the phenomenon is independent on the detailed configuration of the regulator. However, for this case, its RHF is 0.907, which is higher than the regulator with two rows of nanopillars. The spatial distribution of heat flux in P1–P7 is shown in Fig. S5 of the ESM. Therefore, in the heat flux regulator design, increasing the rows of nanopillars, increasing the height of nanopillars, and reducing the host nanofilm thickness, are preferred to obtain high heat flux regulation ratio.

4 Conclusion

In summary, through molecular dynamics calculations, we find that nanophononic metamaterials can realize heat flux regulation. In addition, the height of the nanopillars, the thickness of the host nanofilm, and the number of nanopillars have remarkable impacts on the heat flux regulation ability. The underlying mechanism is the phonon localization of the nanopillars region due to the resonance hybridization effect of the nanopillars and the host material. Furthermore, we found that the metastructures can control heat flux even in the region without nanopillars, through proximity effect. Our work provides theoretical insights into the design and application of nanophononic metastructures.

Declarations The authors declare that they have no competing interests and there are no conflicts.

Data availability statements The data that support the findings of this study are available from the corresponding author upon reasonable request.

Electronic supplementary materials The online version contains supplementary material available at https://doi.org/10.1007/s11467-023-1349-4 and https://journal.hep.com.cn/fop/EN/10.1007/s11467-023-1349-4.

Acknowledgements J. Zhang gratefully acknowledges the financial support from the China Scholarship Council (No. 202206120136).

References

1. J. Chen, J. He, D. K. Pan, X. T. Wang, N. Yang, J. J. Zhu, S. Y. A. Yang, and G. Zhang, Emerging theory and phenomena in thermal conduction: A selective review, *Sci. China Phys. Mech. Astron.* 65(11), 117002 (2022)
2. Y. Liang and J. P. Huang, Robustness of critical points in a complex adaptive system: Effects of hedge behavior, *Front. Phys.* 8(4), 461 (2013)
3. Z. Z. Yu, G. H. Xiong, and L. F. Zhang, A brief review of thermal transport in mesoscopic systems from nonequilibrium Green's function approach, *Front. Phys.* 16(4), 43201 (2021)
4. B. L. Davis and M. I. Hussein, Nanophononic metamaterial: Thermal conductivity reduction by local resonance, *Phys. Rev. Lett.* 112(5), 055505 (2014)
5. H. Honarvar and M. I. Hussein, Two orders of magnitude reduction in silicon membrane thermal conductivity by resonance hybridizations, *Phys. Rev. B* 97(19), 195413 (2018)
6. Z. Wei, J. Yang, K. Bi, and Y. Chen, Phonon transport properties in pillared silicon film, *J. Appl. Phys.* 118(15), 155103 (2015)
7. S. Y. Xiong, K. Saaskilahti, Y. A. Kosevich, H. X. Han, D. Donadio, and S. Volz, Blocking phonon transport by structural resonances in alloy-based nanophononic metamaterials leads to ultralow thermal conductivity, *Phys. Rev. Lett.* 117(2), 025503 (2016)
8. H. Honarvar, L. Yang, and M. I. Hussein, Thermal transport size effects in silicon membranes featuring nanopillars as local resonators, *Appl. Phys. Lett.* 108(26), 263101 (2016)
9. J. Wang, G. Dai, and J. P. Huang, Thermal metamaterial: Fundamental, application, and outlook, *iScience* 23(10), 101637 (2020)
10. D. Yudistira, A. Boes, B. Graczykowski, F. Alzina, L. Y. Yeo, C. M. Sotomayor Torres, and A. Mitchell, Nanoscale pillar hypersonic surface phononic crystals, *Phys. Rev. B* 94(9), 094304 (2016)
11. B. Li, K. T. Tan, and J. Christensen, Tailoring the thermal conductivity in nanophononic metamaterials, *Phys. Rev. B* 95(14), 144305 (2017)
12. X. Wan, D. K. Ma, D. K. Pan, L. N. Yang, and N. Yang, Optimizing thermal transport in graphene nanoribbon based on phonon resonance hybridization, *Mater. Today Phys.* 20, 100445 (2021)
13. H. Wang, Y. Cheng, Z. Fan, Y. Guo, Z. Zhang, M. Bescond, M. Nomura, T. Ala-Nissila, S. Volz, and S. Xiong, Anomalous thermal conductivity enhancement in low dimensional resonant nanostructures due to imperfections, *Nanoscale* 13(22), 10010 (2021)
14. S. Neogi and D. Donadio, Anisotropic in-plane phonon transport in silicon membranes guided by nanoscale surface resonators, *Phys. Rev. Appl.* 14(2), 024004 (2020)
15. S. Q. Hu, L. Feng, S. Cheng, Y. A. Kosevich, and J. Shiomi, Two-path phonon interference resonance induces a stop band in a silicon crystal matrix with a multilayer array of embedded nanoparticles, *Phys. Rev. B* 102(2), 024301 (2020)
16. H. G. Zhang, B. Sun, S. Hu, H. Y. Wang, Y. J. Cheng, S. Y. Xiong, S. Volz, and Y. X. Ni, Novel phonon resonator based on surface screw thread for suppressing thermal transport of Si nanowires, *Phys. Rev. B* 101(20), 205418 (2020)
17. T. Juntunen, O. Vänskä, and I. Tittonen, Anderson localization quenches thermal transport in aperiodic superlattices, *Phys. Rev. Lett.* 122(10), 105901 (2019)
18. Y. Y. Guo, M. Bescond, Z. W. Zhang, S. Y. Xiong, K. Hirakawa, M. Nomura, and S. Volz, Thermal conductivity

minimum of graded superlattices due to phonon localization, *APL Mater.* 9(9), 091104 (2021)
19. R. Anufriev, J. Maire, and M. Nomura, Review of coherent phonon and heat transport control in one-dimensional phononic crystals at nanoscale, *APL Mater.* 9(7), 070701 (2021)
20. Z. W. Zhang, Y. Y. Guo, M. Bescond, J. Chen, M. Nomura, and S. Volz, Coherent thermal transport in nano-phononic crystals: An overview, *APL Mater.* 9(8), 081102 (2021)
21. Y. B. Jin, Y. Pennec, B. Bonello, H. Honarvar, L. Dobrzynski, B. Djafari-Rouhani, and M. I. Hussein, Physics of surface vibrational resonances: pillared phononic crystals, metamaterials, and metasurfaces, *Rep. Prog. Phys.* 84(8), 086502 (2021)
22. J. H. Ma, Phonon engineering of micro- and nanophononic crystals and acoustic metamaterials: A review, *Small Sci.* 3(1), 2200052 (2023)
23. S. Plimpton, Fast parallel algorithms for short-range molecular dynamics, *J. Comput. Phys.* 117(1), 1 (1995)
24. F. H. Stillinger and T. A. Weber, Computer simulation of local order in condensed phases of silicon, *Phys. Rev. B Condens. Matter* 31(8), 5262 (1985)
25. P. F. Zhuang, L. J. Xu, P. Tan, X. P. Ouyang, and J. P. Huang, Breaking efficiency limit of thermal concentrators by conductivity couplings, *Sci. China Phys. Mech. Astron.* 65(11), 117007 (2022)
26. S. Yang, J. Wang, G. L. Dai, F. B. Yang, and J. P. Huang, Controlling macroscopic heat transfer with thermal metamaterials: Theory, experiment and application, *Phys. Rep.* 908, 1 (2021)
27. Z. R. Zhang, L. J. Xu, T. Qu, M. Lei, Z. K. Lin, X. P. Ouyang, J. H. Jiang, and J. P. Huang, Diffusion metamaterials, *Nat. Rev. Phys.* 5(4), 218 (2023)
28. K. A. Dick, K. Deppert, M. W. Larsson, T. Martensson, W. Seifert, L. R. Wallenberg, and L. Samuelson, Synthesis of branched 'nanotrees' by controlled seeding of multiple branching events, *Nat. Mater.* 3(6), 380 (2004)
29. N. Chekurov, K. Grigoras, A. Peltonen, S. Franssila, and I. Tittonen, The fabrication of silicon nanostructures by local gallium implantation and cryogenic deep reactive ion etching, *Nanotechnology* 20(6), 065307 (2009)
30. Z. Huang, X. Zhang, M. Reiche, L. Liu, W. Lee, T. Shimizu, S. Senz, and U. Göselee, Extended arrays of vertically aligned sub-10 nm diameter [100] Si nanowires by metal-assisted chemical etching, *Nano Lett.* 8(9), 3046 (2008)
31. J. M. Dickey and A. Paskin, Computer simulation of the lattice dynamics of solids, *Phys. Rev.* 188(3), 1407 (1969)
32. G. C. Loh, E. H. T. Teo, and B. K. Tay, Phonon localization around vacancies in graphene nanoribbons, *Diamond Related Mater.* 23, 88 (2012)
33. Y. Wang, A. Vallabhaneni, J. N. Hu, B. Qiu, Y. P. Chen, and X. L. Ruan, Phonon lateral confinement enables thermal rectification in asymmetric single-material nanostructures, *Nano Lett.* 14(2), 592 (2014)
34. T. Liang, M. Zhou, P. Zhang, P. Yuan, and D. G. Yang, Multilayer in-plane graphene/hexagonal boron nitride heterostructures: Insights into the interfacial thermal transport properties, *Int. J. Heat Mass Transf.* 151, 119395 (2020)